EUROPEAN ORGANIZATION FOR NUCLEAR RESEARCH

CERN-EP/89-119
14 September 1989

# WA84 EXPERIMENT: A BEAUTY SEARCH WITH A SCINTILLATING-FIBRE MICROVERTEX DETECTOR

WA84 Collaboration

C. Angelini[4], W. Beusch[2], A. Cardini[4], D.J. Crennell[1], M. De Vincenzi[5], G. Di Vita[5], A. Duane[3], J.-P. Fabre[2], V. Flaminio[4], A. Frenkel[5], T. Gys[2], K. Harrison[3], E. Lamanna[5], H. Leutz[2], D. Lucchesi[4], G. Martellotti[5], J.G. McEwen[6], D.R.O. Morrison[2], G. Penso[5], S. Petrera[5], C. Roda[4], A. Sciubba[5], E. Vicari[2] and D.M. Websdale[3]

*Presented by Karl Harrison*

## ABSTRACT

This paper gives a review of the physics aims of the fixed-target experiment WA84, currently being conducted at CERN, and of the methods used. The operation and performance of the scintillating-fibre microvertex detector are described.

Invited talk given at the 4th Pisa Meeting on Advanced Detectors:
Frontier Detectors for Frontier Physics,
La Biodola, Isola d'Elba, Italy, 21–25 May 1989
(To be published in Nuclear Instruments and Methods in Physics Research)

---

1) Rutherford Appleton Laboratory, Didcot, UK.
2) CERN, Geneva, Switzerland.
3) Imperial College, London, UK.
4) Università di Pisa and INFN, Pisa, Italy.
5) Università di Roma 'La Sapienza' and INFN, Rome, Italy.
6) University of Southampton, Southampton, UK.

## 1. INTRODUCTION

The construction of charged-particle tracking devices using scintillating fibres was first undertaken in the late nineteen-fifties, at Imperial College, at the Massachusetts Institute of Technology, and at the Universities of Michigan, Pennsylvania, and Princeton, amongst others. Prototype detectors were assembled from 700 $\mu$m diameter plastic scintillating fibres and were successfully used in recording muon tracks on photographic film [1]. Spatial resolution was, however, poor and there was little further development effort, as the bubble chamber and spark chamber gave excellent results for the applications considered. Interest in the technique was not revived until the early nineteen-eighties [2–4]. By this time improvements in image-intensifier design and in fibre-manufacturing procedures had made the use of the technique in high-energy physics experiments more viable.

The potential of scintillating-fibre devices for providing precise particle tracking in the high-luminosity environments of proposed future high-energy hadron colliders, including the SSC, LHC, and ELOISATRON, has been discussed at length [5, 6]. Whilst work on prototypes of central tracking detectors consisting of concentric cylindrical shells of fibres, intended for such colliders, is currently in progress [7], the use of scintillating fibres for high-resolution tracking (spatial precision $\leq 25$ $\mu$m) is at present restricted to fixed-target geometries.

The WA84 Collaboration at CERN proposes to use a scintillating-fibre active target as a microvertex detector, to be installed in the Omega Prime spectrometer facility [8], for the study of the hadroproduction and decay of mesons containing the beauty (b) quark [9]. This paper contains a review of the physics aims and a description of the experimental set-up, but is mainly concerned with the operation and performance of the microvertex detector.

## 2. WA84 EXPERIMENT

The aim of the WA84 experiment is to permit full reconstruction of a large sample of events in which the creation and decay of B and $\overline{\mathrm{B}}$ mesons (containing, by convention, the $\bar{\mathrm{b}}$ and b quarks, respectively) is observed, with the four heavy-flavour decay vertices to be detected in about one third of the events. From this sample, it would be possible for the lifetimes of the charged and neutral states of the B meson to be determined separately, the two being different if non-spectator effects contribute significantly to the decay process, as is the case for charm decays. The recording of all decay vertices would enable direct measurement of the branching ratios for decays of the b quark to u and c quarks, giving knowledge of currently indeterminate elements of the Cabibbo–Kobayashi–Maskawa matrix. An evaluation of mixing in the $\mathrm{B_s}$–$\overline{\mathrm{B}}_\mathrm{s}$ system, predicted to be near-maximal by the Standard Model, would be made.

The layout for the experiment is shown in Fig. 1. A high-intensity beam ($\sim 1.5 \times 10^6$ particles per burst) of 350 GeV/c negatively charged pions is incident on an active target, typically having a length of 50 mm and a cross-section of $5 \times 5$ mm$^2$, composed of narrow-diameter ($\leq 30$ $\mu$m) scintillating fibres. The target is positioned in the field of the Omega magnet and aligned so that the fibre axes are parallel to the beam direction, providing light images of events projected onto the plane which is transverse to the beam direction (Fig. 2). Following amplification by a gateable optoelectronic chain, the image of a triggered event is stored on a charge-coupled device (CCD) of $550 \times 288$ pixels until completion of the readout, performed at a rate of 15 MHz (although so far tested only at 4 MHz). The silicon microstrip detector used is the one assembled by the WA82 Collaboration [10], operated with six planes located upstream of the target and thirteen planes placed downstream. It allows the determination of vertex positions along the beam direction and assists in the matching of tracks seen in the target with those for which the associated momenta are measured in the multiwire proportional chambers of the Omega Prime spectrometer. Off-line particle

identification is aided by the information provided by the ring-imaging Cherenkov detector (RICH) [11] and by the electromagnetic calorimeters used for photon detection [12].

A two-level trigger is implemented to select the events to be written to tape. The first-level trigger, which uses small scintillation counters placed close to the target, is for interactions, with a decision time of ~ 100 ns. The second-level trigger makes use of a pair of so-called butterfly hodoscopes, installed in the spectrometer, and one of the wire chambers to select events in which at least four particles with transverse momentum greater than 600 MeV/c are produced, with a decision time of ~ 400 ns. For an initial beam flux of ~ $1.5 \times 10^6$ particles per burst, the acceptance is ~ $10^5$ interactions per burst after the first-level trigger and ~ 60 events per burst following the second-level trigger. These acceptances have been measured experimentally, and the final rate is compatible with that which is allowed when considering the time needed for readout of the target information from the CCD (~ 11 ms). Monte Carlo simulations show that, for a plastic-fibre target, the trigger enriches the beauty signal over the background by a factor of ~ 200. Assuming that there is a cross-section of 5 nb per nucleon for beauty production and linear A-dependence, this indicates that the number of B–$\overline{\text{B}}$ decays recorded is about 1 per $1.2 \times 10^4$ events or, for an accelerator cycle giving three bursts every minute, 30 per day. Extraction of the B–$\overline{\text{B}}$ signal requires automatic vertex recognition for the events in the target. An estimated 0.5% of events in which there are three or more secondary vertices will be beauty decays.

## 3. THE SCINTILLATING-FIBRE TARGETS

A number of scintillating-fibre targets have been tested, differing from one another in features such as fibre size, nature of scintillator (either glass or plastic), and method of target fabrication. In all cases, the design is essentially the same. The basic target is constructed from tens of thousands of scintillating microfibres, first assembled as coherent bundles. It has a cross-section of the order of $5 \times 5$ mm$^2$ and a length of a few centimetres. This allows sufficient material for the observation of the B–$\overline{\text{B}}$ decays without there being too high a number of secondary interactions. An individual fibre consists of a scintillating core, occupying about 70% of the total volume, and an inactive cladding of lower refractive index. With glass, it has been possible to make fibres that are square in cross-section, thus maximizing the packing fraction. Manufacturing of plastic fibres is not yet so advanced. For these, the initially circular cross-section is made almost perfectly hexagonal by the deforming forces to which the fibres are subjected during the pulling and heating that are required in the course of target production. The separation of parallel sides of the core cross-section (sometimes referred to as the core diameter) has ranged from 15 $\mu$m to 30 $\mu$m for the different fibres tested, and the cladding thickness has been between 1.5 $\mu$m and 3.0 $\mu$m. Photographs of end views of two of the targets, illustrating the excellent geometrical arrangement of the fibres, are shown in Fig. 3.

Event images are formed by light, generated isotropically along the path of a charged particle, being trapped by internal reflection in a single fibre and transmitted to the target end. For fibres to be useful, the light emission and trapping must occur within a distance that is small compared with the fibre diameter. This requirement of local emission imposes restrictions on the choice of scintillator for the microfibre core.

A scintillator consists of a base material and at least one dopant. Ionizing particles excite the molecules of the base, which undergo radiative decay with low probability (for example, ~ 4% for glass and ~ 3% for polystyrene). In order to increase the light yield, a primary solute is added, for which non-radiative transfer of energy from the base, via the Förster mechanism [13], is favoured, and for which subsequent radiative decay takes place with a large probability (> 60%). Such light emission, referred to as primary emission, is inevitably highly localized. If the absorption and emission spectra of the primary solute are sufficiently well separated to allow the light to be transmitted without it being too greatly attenuated, then no other dopants are necessary, and the

trapping is as shown in Fig. 4. This is the case for the cerium-doped GS1 scintillator glass[1], containing 3% (by weight) $Ce_2O_3$, which was the core material for the first fibres tested. For primary solutes commonly used in plastic scintillators, there is considerable overlap of the absorption and emission spectra. The light transmission properties are improved by adding a second solute, known as a wavelength shifter (WLS), which absorbs the primary light and gives secondary emission at longer wavelengths. A discussion of the effects of dopant concentrations on light yield and attenuation lengths may be found in Ref. [14]. For efficient trapping in fibres, the mean free path of the primary light must be small relative to the fibre diameter (Fig. 5). Plastic scintillators with standard dopant concentrations [for example, polystyrene doped with 1% (by weight) 2-phenyl-5-(4-biphenyl)-1,3,4-oxadiazole (PBD) as the primary solute, and 0.01% (by weight) p-bis[2-(5-phenyloxazoyl)]benzene (POPOP) as WLS] are inappropriate for microfibres because the primary light has a mean free path of $\geq$ 250 $\mu$m. It is only very recently that plastic scintillators that are suitable for such narrow fibres have been produced. Plastic microfibres tested have had cores of SCSN-81T (0.50)[2], having 20 times the standard concentration of WLS (resulting in a mean free path for the primary light of $\sim$ 10 $\mu$m) or of polystyrene doped with 1-phenyl-3-mesityl-2-pyrazoline (PMP)[2], for which the large Stokes' shift [15] permits satisfactory light transmission without the need for an added WLS.

The fraction of the emitted light trapped in a fibre by internal reflection is dependent on the ratio of the indices of refraction of core and cladding materials and on the geometry of the core cross-section. For the fibre types considered, this fraction represents $\leq$ 4% in each direction along the fibre. Untrapped light can generate optical noise, termed cross-talk, so that every fibre should, ideally, be coated with a thin layer of opaque material, referred to as an extra-mural absorber (EMA), preventing the passage of light between adjacent fibres. This has been possible with glass fibres, although the absorption efficiency of the EMA is quite low, but not with plastic fibres where, so far, it has only been possible to coat 0.5 $\times$ 0.5 mm$^2$ bundles of fibres with an EMA before target assembly.

Both the glass and the plastic materials used may receive doses of at least $10^3$ Gy with little deterioration in transmission properties. Indeed, it has been shown [16] that the GS1 glass is particularly resistant to radiation, and that even when damage is sustained from high doses ($\sim 10^6$ Gy) the original performance may be largely recovered by annealing at 400°C. However, the WA84 Collaboration has measured long-lived components that are of significant intensity for the GS1 light emission [17], previously reported to be fast only [16, 18]. These lead to the superposition of event images that are generated within less than $\sim$ 100 $\mu$s of one another, limiting the beam luminosity that may be used in an experiment to $\sim 10^3$ particles per second. This is too low for the WA84 experiment. No problems of time response have been found for the plastic fibres (all light emitted in some tens of nanoseconds).

The alignment of the target with the fibre axes parallel to the beam direction has been chosen because of the nature of the events to be studied. In a B-$\bar{\text{B}}$ decay, a high multiplicity of tracks is expected, evenly spread over 360° in the plane transverse to the beam line, as in the Monte Carlo simulation of Fig. 6. The mean distance travelled by a beauty particle in this plane before decay is about 400 $\mu$m. Many particles will travel at small angles to the beam direction, leading to an average Lorentz factor enhancement of $\sim$ 10 in the scintillation yields along their paths (Fig. 7).

---

1) Levy Hill Laboratories, Ltd., 5 Sheffield House, Fieldings Road, Cheshunt, Waltham Cross, Herts. EN8 9TJ, UK.

2) Kyowa Gas Chemical Industry Co., Ltd., Shuwa Higashi-Yaesu Building, 1-Go, 9-Ban, 2-Chome, Hatchobori, Chuo-ku, Tokyo 104, Japan.

## 4. THE OPTOELECTRONIC CHAIN

When the light image generated at the target surface arrives at the CCD for readout, it has been intensified many times during its transmission along the optoelectronic chain of Fig. 8. Transportation of the image from the beam line is achieved using a glass-fibre bent taper which, in addition, introduces a magnification of 3.4 that helps preserve the spatial resolution. Initial, low-level, image intensification is performed by two proximity-focused image intensifiers (proxifiers)[3], $II_1$ and $II_2$, operated with their faceplates perpendicular to the direction of the Omega magnetic-field vector. For minimum-ionizing particles, with the exception of those travelling at very small angles with respect to the beam direction, the light from a single fibre is sufficient to release, at most, only one photoelectron at the bialkali photocathode of the first proxifier, for which the quantum efficiency is about 0.16, after taking into account the losses at the input window. The second proxifier is provided with an especially thick input window, for insulation purposes. Total gain for the two proxifiers is around 1000 photons per detected photoelectron. This compensates for the factor of $\sim$ 10 attenuation that is suffered when the image is transported, via a 2.5 m long image-guide[4] of 10 $\mu$m fibres, to a region of no magnetic field, where the stronger light amplification may take place. Most of this light amplification ($\sim$ 1000 photons per photon) is performed by a gateable microchannel plate (MCP) image intensifier[5], $II_4$. The spatial resolution of this type of image intensifier is poor, so that the image is magnified as much as possible before entering the MCP, using an electrostatically focused image intensifier[6], $II_3$. A second electrostatically focused image intensifier[7], $II_5$, demagnifies the image after the MCP, to match the size of the CCD[8], which has a quantum efficiency of $\sim$ 0.20. Both electrostatically focused image intensifiers introduce additional small gains ($\sim$ 6 photons per photon for each). Gains and magnifications of the various components of the optoelectronic chain are summarized in Table 1.

The bent taper used in piping the image from the beam line is eventually damaged by the radiation levels for high luminosity. Recent tests have been made with the bent taper replaced by a system of a mirror and seven-element lens[9], offering radiation hardness. This lens–mirror system is comparable in spatial resolution to the bent taper and has a slightly higher transmission efficiency for the scintillation light of the targets tested.

Triggering of the optoelectronic chain is made possible by virtue of the fact that the MCP image intensifier can be gated. When the first-level trigger is satisfied, the potential of the S20 photocathode is made lower than that of the input face of the MCP, allowing the free passage of photoelectrons through the image intensifier. The decay-times of the phosphors in the image intensifiers preceding the MCP are long enough to ensure that none of the photoelectrons produced in the first proxifier are undetected because of the time taken ($\sim$ 100 ns) in implementing the trigger. The gated-on mode is maintained for $\leq$ 1 $\mu$s to allow the amplified event image to be detected at the P47 phosphor of the MCP image intensifier. This is sufficient for the plastic scintillators (where the temporal dispersion of

---

3) Proxitronic GmbH, Robert Bosch Strasse 34, 6140 Bensheim, Federal Republic of Germany.

4) Schott Fiber Optics, Inc., 122 Charlton Street, Southbridge, MA 01550, USA.

5) ITT, Electro-optical Products Division, 3700 East Pontiac Street, PO Box 3700, Fort Wayne, IN 46801, USA.

6) Varo, Inc., Electron Devices Division, 2203 Walnut Street, PO Box 469014, Garland, TX, USA.

7) B.V. Delft Electronische Producten, Postbus 60, Dwazziewegen 2, 9300 AB Roden (Dr.), The Netherlands.

8) Thomson-CSF, Division Tubes électroniques, 38 rue Vauthier, BP 305, 92102 Boulogne-Billancourt Cedex, France.

9) Cerco, Z.A. de Courtabœuf, avenue de la Baltique, 91951 Les Ulis Cedex, France.

the signal is dominated by the phosphor decay-times) but not for the cerium-doped GS1 with the long-lived components of the light emission. The MCP is then gated-off by making the voltage at the entrance to the MCP more negative than the potential at the photocathode, thus preventing further input. A similar gating procedure is used in the triggering of the scintillating-fibre detector in the upgraded UA2 detector [19].

The CCD has an image zone and a memory zone, each of 550 × 288 pixels with dimensions 16 $\mu$m × 23 $\mu$m. If the second-level trigger is satisfied, the event initially recorded on the image zone is transferred to the memory zone, in an operation which is completed in about 150 $\mu$s. Otherwise, a Fast Clear of the image zone is performed, using the antiblooming facility of the CCD [20], in about 1 $\mu$s. Pixel addresses and pulse heights are read from the memory zone and written to tape, following zero suppression by a data compactor module (DCM) which reduces the quantity of data to ~ 30 Kbytes (with 4 bytes per pixel) for a typical interaction.

## 5. TEST RESULTS

Extensive tests of the scintillating-fibre microvertex detector and optoelectronic chain have been carried out. These have involved laboratory studies of the sources of noise [21], of the time response, and of the dependence of the light-detection efficiency on the gains of the different image intensifiers [22], as well as data-taking in particle beams at the CERN Proton Synchrotron (PS) and Super Proton Synchrotron (SPS). At the test beams, both single-particle tracks and interactions have been recorded.

For the cerium-doped GS1 glass fibres, the most significant result has come from measurements of the long-lived components of the light emission [17]. These show that the fast component (decay time of 71 ns) accounts for less than 40% of the total light and that emission continues for more than 1 ms, so that the GS1 fibres cannot be used with the beam intensity (~ $1.5 \times 10^6$ particles per burst) that is required to achieve a reasonable rate for the WA84 experiment. However, other results obtained from the analysis of event images obtained with the glass targets, and particularly those that relate to the effect of the EMA, remain informative.

Most of the single-particle tracks are recorded under slightly non-standard conditions, with the target tilted with respect to the beam line, typically by either 12° or 20°, so that the particle enters and leaves through the target sides (rather than through its ends), producing straight-line images at the readout face, as shown in Fig. 9. Analysis of these track images is used in assessing different targets. A comparison of the performances of glass and plastic active targets, based on such analysis, is presented elsewhere [23], but results are summarized here. The light integration time considered is 4 $\mu$s for glass fibres (allowing the recording of about ~ 70% of the information) and 1 $\mu$s for plastic fibres (believed to allow the recording of all information).

Tracks are defined by series of clusters of contiguous pixel-hits (pixels having non-zero pulse heights) on the CCD. Under the experimental conditions selected, each of these clusters, referred to as a hit, is due to a single photoelectron released at the photocathode of the first image intensifier. Straight lines can be fitted to the hits (or pixel-hits) and then, for many tracks superimposed on one another, the distribution of pulse height transverse to the (projected) track direction is plotted (Fig. 10). After background subtraction, a Gaussian is fitted to the distribution, from which the root-mean-square value for the two-track resolution, $\sigma_{TT}$, is calculated. This depends both on the spatial extent of the hits and on their distribution about the track. For the plastic fibres tested, having 30 $\mu$m diameter cores of either SCSN-81T(0.50) or PMP-doped polystyrene, the value of $\sigma_{TT}$ is ~ 20 $\mu$m in all cases. A similar resolution is found for fibres with a 25 $\mu$m cerium-doped GS1 core and for plastic fibres with a 15 $\mu$m core, possibly suggesting that current manufacturing processes introduce slightly greater target incoherence (image distortion due to non-perfect parallel alignment

of microfibres) for the narrower diameters. For plastic fibres with a 50 $\mu$m core there is a slight worsening of resolution, giving $\sigma_{TT} \approx 25$ $\mu$m.

The hit density is defined by the ratio of the number of hits within $3\sigma_{TT}$ of a fitted track to the (known) path length of the particle that generates the hits. Hit densities measured experimentally depend on the quantity of light initially trapped, on the degree of light attenuation in the target, and on losses in the optoelectronic chain. For comparative purposes, representative values of the hit density are obtained by considering particles which pass approximately through the target centre. The hit densities then found are [23] 0.6 $mm^{-1}$ for 25 $\mu$m GS1 fibres; 1.4 $mm^{-1}$ for 30 $\mu$m SCSN-81T(0.5) fibres; 1.6 $mm^{-1}$ for 30 $\mu$m fibres with a core of polystyrene doped with 1.5% (by weight) PMP. Variations in the measured hit densities are due to differences in the light-attenuation lengths rather than dissimilarities in the scintillation yields (a minimum-ionizing particle generating $\sim$ 2300 photons per mm in the glass, integrating over all light, and $\sim$ 1800 photons per mm in the plastics). The attenuation lengths found experimentally, which depend both on light absorption within the material and on reflection losses at the core–cladding interface, are [23] 2.0 cm in the GS1 fibres, 9.4 cm in the SCSN-81T(0.50) fibres, and 30.8 cm in the PMP fibres. With a mirrored surface positioned at the non-readout end of the target composed of PMP fibres, the hit density is increased to 2.3 $mm^{-1}$. Little increase is found for the target of SCSN-81T(0.50) fibres, and none for the glass target, because of the shorter attenuation lengths. There is some evidence that reducing the concentration of the PMP from 1.5% to 0.7% (by weight) marginally decreases the hit density. No gains (or losses) in the hit density have been detected for fibres containing 3% (by weight) PMP.

Light detected more than $3\sigma_{TT}$ from a fitted track is attributed to some form of noise. The amount of noise present on an image frame can be considerable, accounting for as much as 48% of all light detected when using a plastic-fibre target with no EMA of any kind, in the absence of magnetic field. From the distribution of pulse height transverse to the (projected) track direction (Fig. 10), it is evident that the noise is spread over a large area, although it is more concentrated at smaller distances from the track. Experimental and theoretical studies have led to the identification of three sources of noise [21]. Monte Carlo simulations show that the physical phenomenon of delta-ray production (approximately the same for the GS1 and for the plastics) contributes to the noise about 10% of the total light on an image frame. The other two types of noise are associated with instrumentational effects, arising from the back-scattering of photoelectrons at the phosphor of the first image intensifier (whereby hits are displaced from tracks) and optical cross-talk (given by scintillation light detected in a fibre other than that in which the primary emission occurs). Measurements show that about 12% of electrons are back-scattered in the first image intensifier. The back-scattering process cannot be suppressed, but the maximum distances by which the electrons can be displaced, as measured at the target surface, is decreased by applying a strong magnetic field perpendicular to the faceplates of the proxifiers (as in the WA84 standard set-up) and by having large magnification between target and proxifier, so that the effect becomes unimportant. Other noise is attributed to cross-talk and is lessened by the use of EMA. The contribution of the noise to the total light detected using a plastic target, in the absence of magnetic field, is reduced from 48% to 40% when the outer surface is coated with an EMA (eliminating the light which is untrapped in the fibres but internally reflected at the plastic–air boundary) and to 25% when the target is assembled from 0.5 mm $\times$ 0.5 mm EMA-coated fibre bundles. Cross-talk is still present in glass targets, where the measured noise is 27% of all detected light, indicating that the EMA on the individual fibres is not perfectly opaque. Doubling the amount of EMA on each fibre produces only a slight additional decrease in cross-talk [22]. Diffusion of the EMA layer into the fibre cladding can result in an inferior hit density.

Examples of high-energy interactions are shown in Fig. 11. The lower hit density for the target of GS1 fibres is evident. With the target assembled from EMA-coated bundles there are, at present,

occasional breaks in tracks when a particle passes through a layer of EMA. Improvements stemming from increased experience in constructing such targets are expected to lead to the disappearance of these gaps. It should be noted that, in the event image reproductions, only the information concerning the positions of the pixel-hits is retained. Pulse heights are lost, so that the spatial resolution is not truly represented. When colours are used to display different ranges of pulse height, structure is found in the region about the primary vertex which, as printed, appears uniformly black. Tracks can be seen and the position of the primary vertex can generally be determined, to within one or two fibre diameters, by searching for the group of 3 $\times$ 3 pixels having greatest pulse height. Reconstruction of tracks from the primary vertex is based on a knowledge of the angular distribution of pulse height about the vertex. For the reconstruction of secondary vertices, an algorithm that uses the Hough transform [24] is being studied.

## 6. CONCLUSIONS

Particle tracks and interactions have been recorded using the WA84 scintillating-fibre microvertex detector. Tests of the optoelectronic chain used for intensifying the image and transferring it to the CCD for readout have shown it to be reliable and efficient. The scintillating-fibre targets allow high spatial precision, with a two-track resolution corresponding to $\sigma_{TT} \approx 20$ $\mu$m. Whilst the GS1 glass fibres cannot be used for the WA84 experiment, because of the intense long-lived components of the light emission and the short light-attenuation length, results for the newly developed plastic fibres, and in particular for the PMP-doped polystyrene fibres, are promising. For a target of PMP fibres, a light-attenuation length of $\sim$ 30 cm has been measured, resulting in a hit density of 2.3 $mm^{-1}$ (representative value) with a mirrored surface placed at the non-readout end. Levels of noise are being steadily reduced, and if the current progress is maintained then the technique of particle tracking with scintillating fibres should soon be producing physics results.

**Acknowledgements**

The continued support of Drs. H. Wenninger and J.C. Gouache, EF Division, CERN, is gratefully acknowledged.

We are indebted to the engineers and technicians of the EF Instrumentation Group at CERN who have contributed to this work, and in particular to J. Dupont and J. Dupraz for their constant involvement and to D. Piedigrossi who assembled the plastic targets. In addition, we thank the physicists of the Birmingham group of the WA77 Collaboration who helped with the first full tests in the Omega Prime spectrometer, and F. Antinori (CERN) and R. Hurst (Genoa) for much valued assistance with the microstrips.

## REFERENCES


[1] G.T. Reynolds, IRE Trans. Nucl. Sci. **NS-7** (1960) 115.

[2] S.R. Borenstein and R.C. Strand, Proc. 1981 ISABELLE Workshop (Brookhaven report BNL-51443, New York, 1981), p. 1438.

[3] L.R. Allemand et al., Nucl. Instrum. Methods **A225** (1984) 522.

[4] R. Ruchti et al., IEEE Trans. Nucl. Sci. **NS-30** (1983) 40 and **NS-31** (1984) 69.

[5] D. Binnie et al., Proc. DPF Summer Study on the Design and Utilization of the Superconducting Super Collider, Snowmass, Colo., 1984 (Amer. Inst. Phys., New York, 1985), p. 593.

[6] C. D'Ambrosio et al., preprint CERN-EP/89-44 (1989), talk given at the Workshop on Scintillating Fiber Development for the SSC, Batavia, Ill., 1988 (FNAL, Batavia, Ill., 1989), p. 611.

[7] H. Leutz, ICFA Instrumentation Bulletin **6** (1989) 6.

[8] W. Beusch et al., technical report CERN/SPSC 77-70, SPSC/T-17 (1977).

[9] W. Beusch et al., proposal CERN/SPSC 87-2, SPSC/P 226 (1987).

[10] J.F. Baland et al., Nucl. Phys. B (Proc. Suppl.) **1B** (1988) 303.

[11] R.J. Apsimon et al., IEEE Trans. Nucl. Sci. **NS-34** (1987) 504.

[12] R. Oedingen, Bonn Univ. preprint BONN IR 84-14 (1984).

[13] T. Förster, Ann. Physik **2** (1948) 55.

[14] A. Grimes et al., Northeastern Univ. preprint NUB-2943 (1988).

[15] P. Destruel et al., Nucl. Instrum. Methods **A276** (1989) 69.

[16] M. Atkinson et al., Nucl. Instrum. Methods **A254** (1987) 500.

[17] C. Angelini et al., Nucl. Instrum. Methods **A281** (1989) 50.

[18] R. Ruchti et al., IEEE Trans. Nucl. Sci. **NS-33** (1986) 151.

[19] J. Alitti et al., Nucl. Instrum. Methods **A279** (1989) 364.

[20] S. Reynaud, CERN/EF/INSTR 86-1 (1986).

[21] C. Angelini et al., preprint CERN-EP/89-120, presented by G. Penso at this conference.

[22] C. Roda, Tesi di laurea, Univ. Pisa, 1989 [Report CERN/EF/INSTR 89-1 (1989)].

[23] C. Angelini et al., preprint CERN-EP/89-112 (1989), submitted to Nucl. Instrum. Methods.

[24] R.O. Duda and P.E. Hart, Commun. ACM **15** (1972) 11.

**Table 1**

Gain and magnification factors for components of the optoelectronic chain, under standard operating conditions

| Component | Photocathode | Phosphor | Gain ($\gamma$ per $\gamma$) | Magnification |
|---|---|---|---|---|
| Bent taper | | | ~0.4 | 3.4 |
| $II_1$ | Bialkali | X3 | ~130.0[a)] | 1.0 |
| $II_2$ (with thick input window) | Bialkali | X3 | ~8.0 | 1.0 |
| Image guide (2.5 m in length) | | | ~0.1 | 1.0 |
| $II_3$ | S20 | P47 | ~6.0 | 1.8 |
| $II_4$ | S20 | P47 | ~1000.0 | 1.0 |
| $II_5$ | S20 | P46 | ~6.0 | 0.2 |

a) Approximate gains in photons per photon are given except for the first image intensifier, where it is the gain in photons per photoelectron which is important. The quantum efficiency for the photocathode of $II_1$ is about 0.16, after allowing for the transmission of the input window. An estimated 60% of electrons released at the photocathode of $II_1$ are detected at the phosphor.

**Figure captions**

Fig. 1 Layout for CERN experiment WA84. A beam of 350 GeV/c $\pi^-$ particles is incident on the scintillating fibre (SCIFI) target. Matching of tracks seen in the target with those recorded in the multiwire proportional chambers (MWPCs) of the spectrometer is aided by the silicon microstrip detector (MSD) system. The ring-imaging Cherenkov detector and photon detector are used for off-line event reconstruction.

Fig. 2 Alignment of target to provide event images projected onto the plane that is transverse to the beam direction.

Fig. 3 End views of sections of targets constructed from fibres having a cerium-doped GS1 glass core (top) and from fibres having a PMP-doped polystyrene core (bottom). Either the core or cladding appears white, depending on the position of the light source used for illumination. One of the boundaries between fibre bundles may be seen in the case of the glass target. A slight deformation is apparent for some of the fibres in the plastic target.

Fig. 4 Trapping of light following primary emission.

Fig. 5 Trapping of wavelength-shifted light following secondary emission.

Fig. 6 Monte Carlo simulation of B–$\overline{\text{B}}$ production and decay, viewed in the plane transverse to the beam line. In addition to the primary interaction vertex, the four decay vertices are seen.

Fig. 7 Lorentz factor light enhancement.

Fig. 8 Gated optoelectronic chain used in transporting the event image at the surface of the scintillating fibre (SCIFI) target out of the beam line and away from the magnetic field, providing amplification of the light so that it can be recorded at the CCD.

Fig. 9 Track images for 6 GeV hadrons, passing approximately through the target centre, with fibre axes at 20° with respect to the beam line: a) in a target of fibres with cores of cerium-doped GS1 glass, each coated with an EMA; b) in a target of fibres with cores of polystyrene doped with 3% (by weight) PMP, mirrored surface at non-readout end, EMA on outer target surface only; c) in a target of fibres with cores of polystyrene doped with 0.7% (by weight) PMP, assembled from 0.5 mm × 0.5 mm EMA-coated bundles.

Fig. 10 Distribution of pulse height transverse to (projected) track direction, shown for a target of fibres with cores of polystyrene doped with 1.5% (by weight) PMP, EMA on target surface only, fibre axes at 20° with respect to the beam line.

Fig. 11 Interactions recorded with the target parallel to the beam direction: a) 340 GeV $\pi^-$ in a target of fibres with cores of cerium-doped GS1 glass, each coated with an EMA; b) 200 GeV hadron in a target of fibres with cores of polystyrene doped with 3% (by weight) PMP, mirrored surface at non-readout end, EMA on outer target surface only; c) 200 GeV hadron in a target of fibres with cores of polystyrene doped with 3.0% (by weight) PMP, assembled from 0.5 mm × 0.5 mm EMA coated bundles.

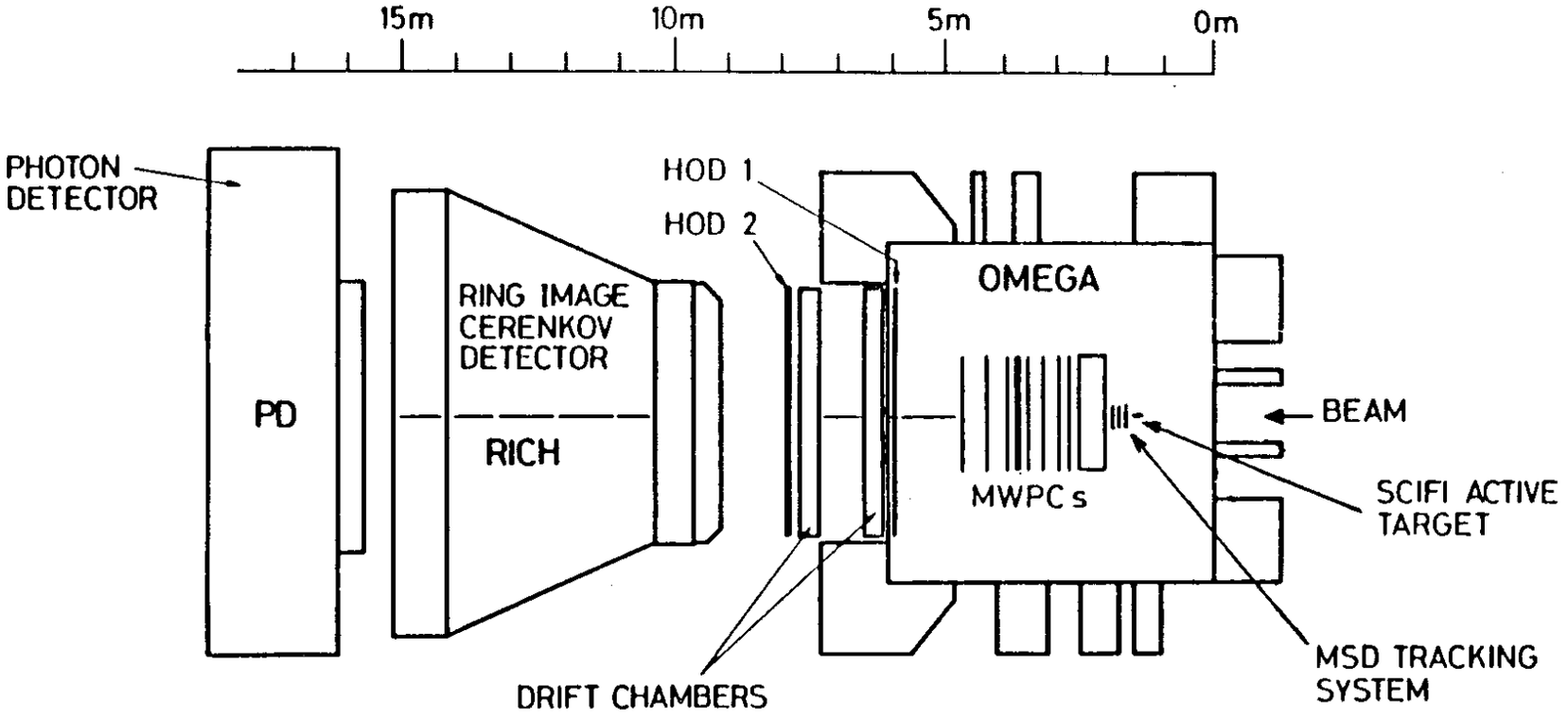
15m
10m
5m
0m
PHOTON DETECTOR
PD
RING IMAGE CERENKOV DETECTOR
RICH
HOD 1
HOD 2
OMEGA
MWPCs
BEAM
SCIFI ACTIVE TARGET
MSD TRACKING SYSTEM
DRIFT CHAMBERS

**Fig. 1**

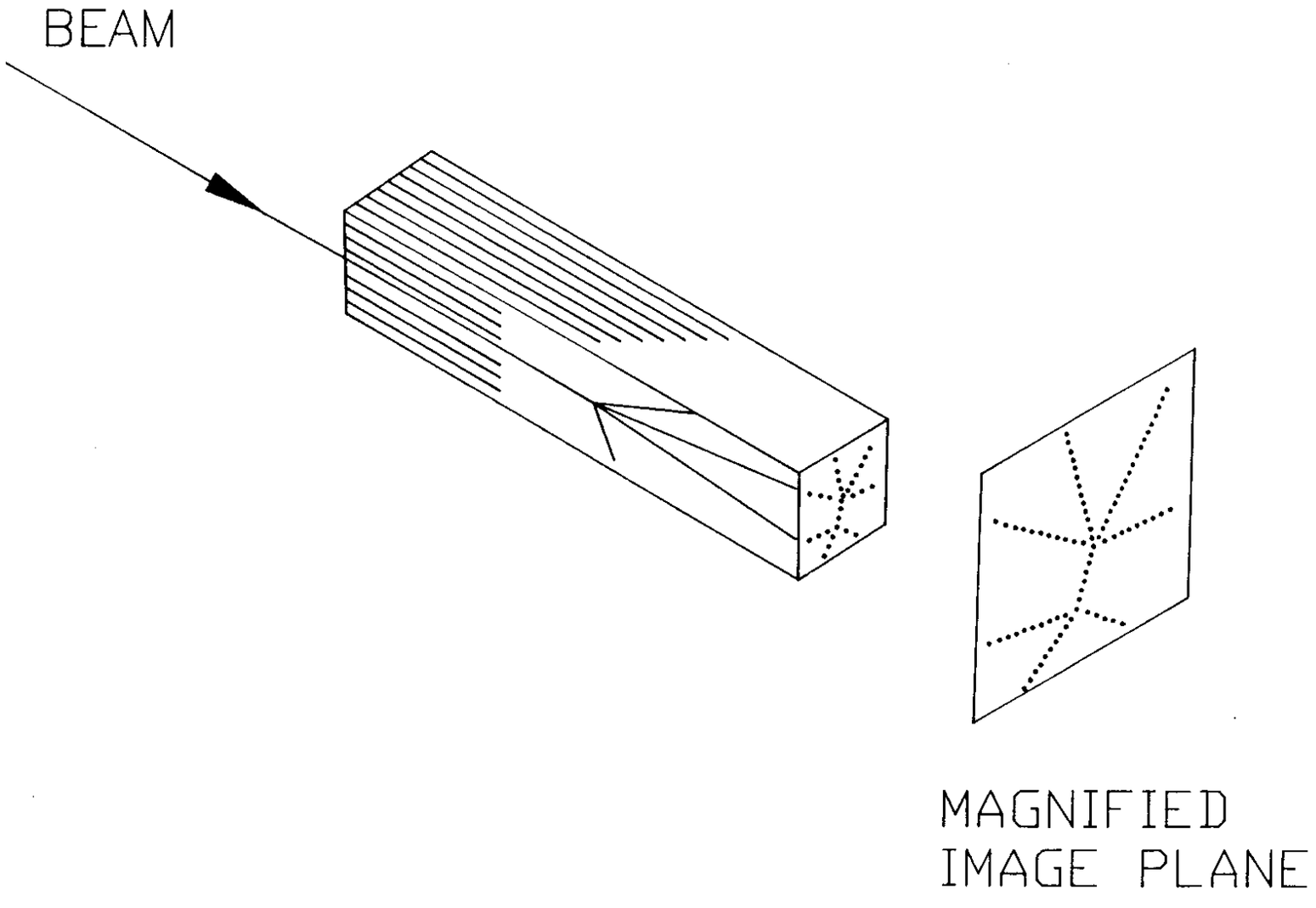


**Fig. 2**

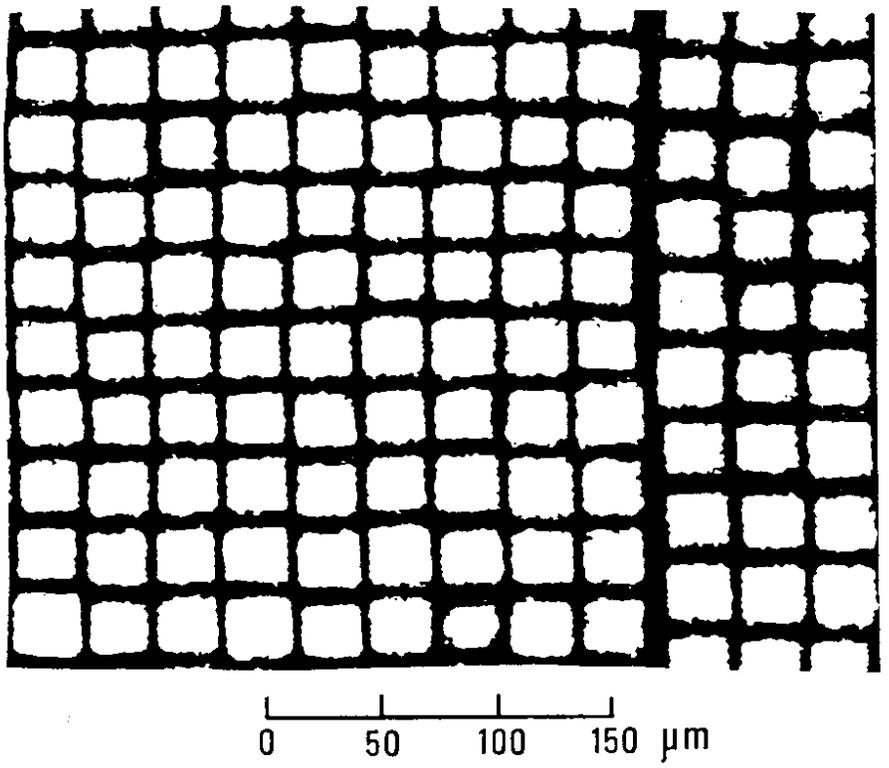


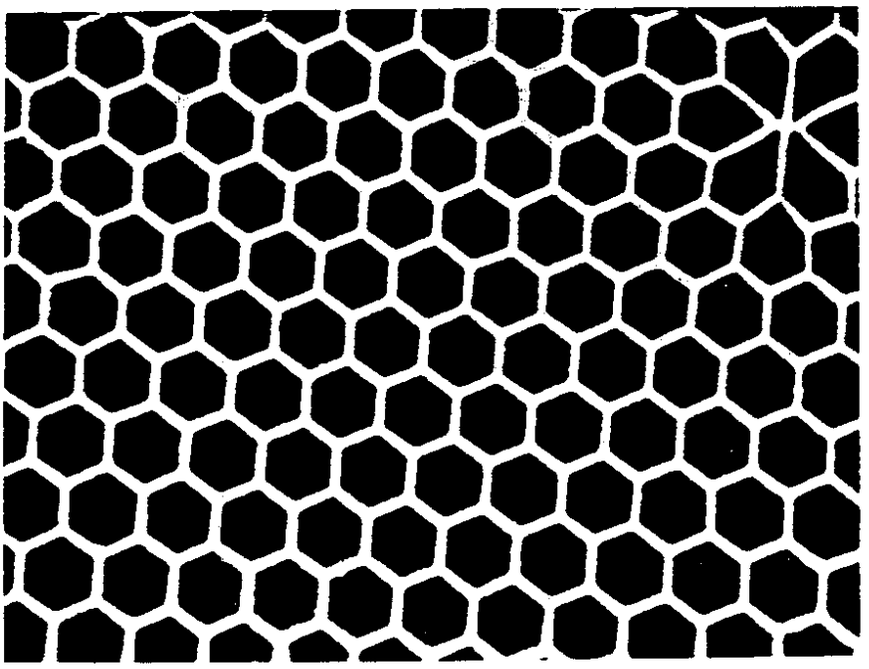

Fig. 3

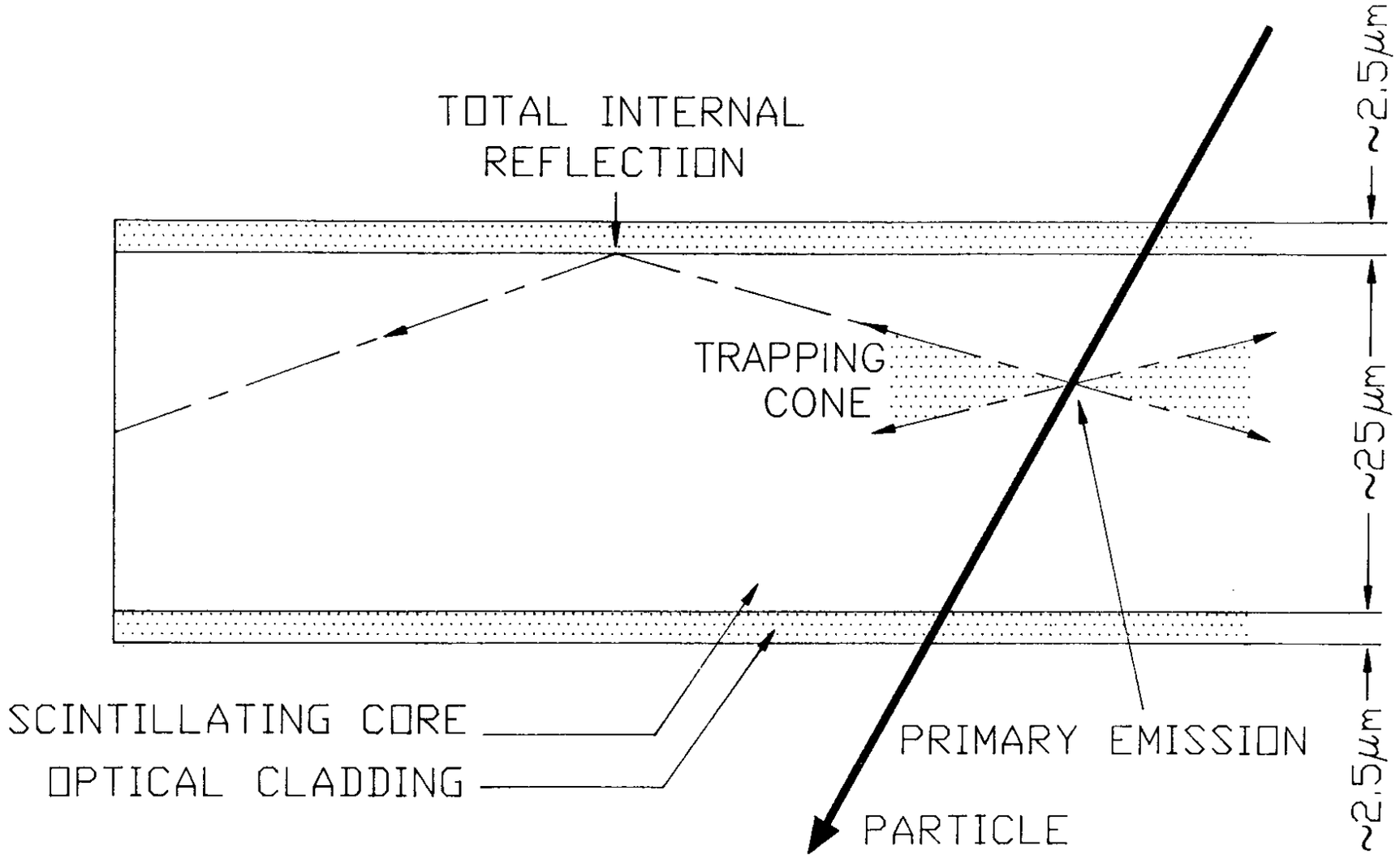
TOTAL INTERNAL
REFLECTION
TRAPPING
CONE
SCINTILLATING CORE
OPTICAL CLADDING
PRIMARY EMISSION
PARTICLE
~2.5μm
~25μm
~2.5μm

**Fig. 4**

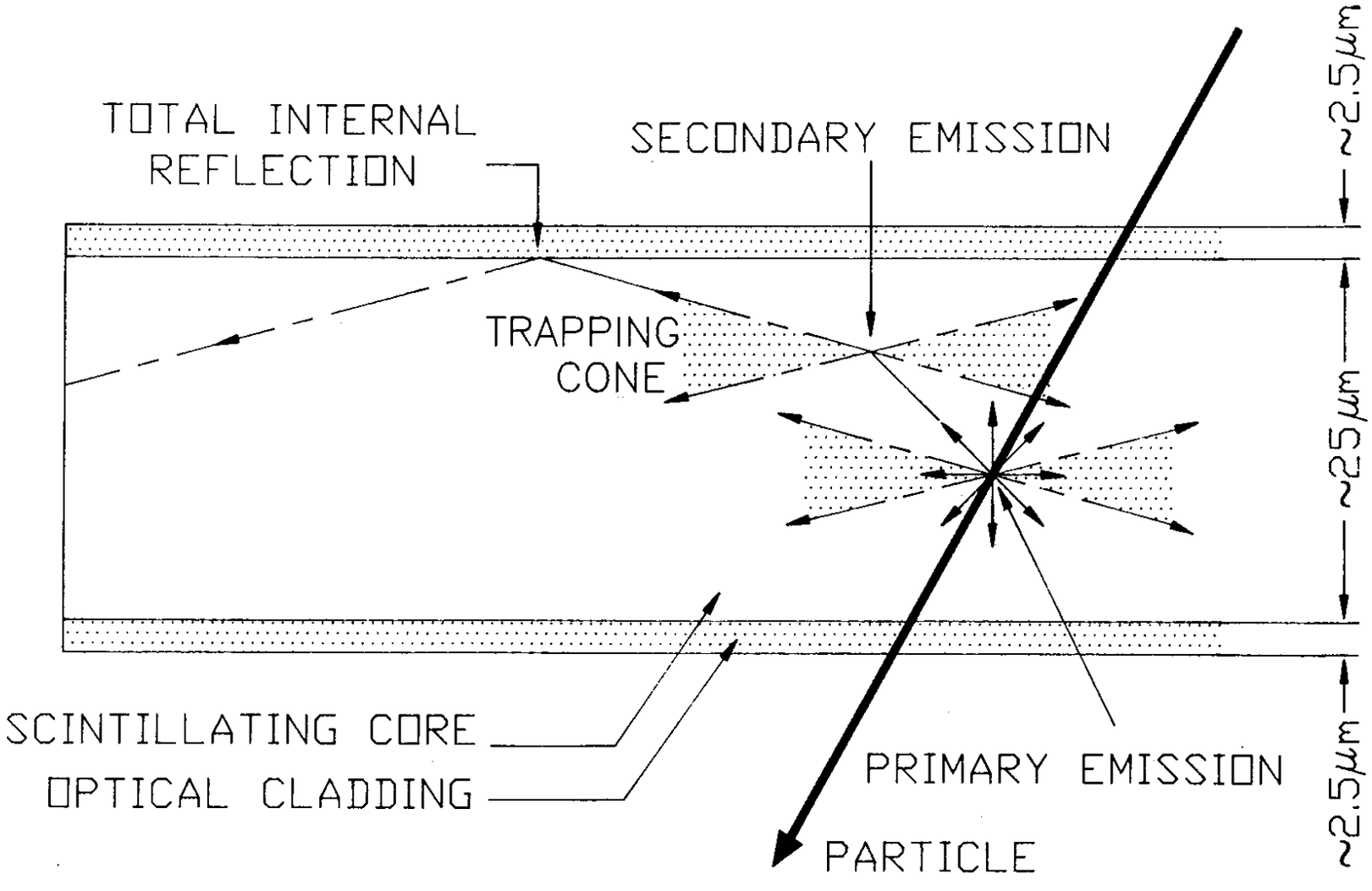
TOTAL INTERNAL
REFLECTION
SECONDARY EMISSION
~2.5μm
TRAPPING
CONE
~25μm
SCINTILLATING CORE
OPTICAL CLADDING
PRIMARY EMISSION
PARTICLE
~2.5μm

**Fig. 5**

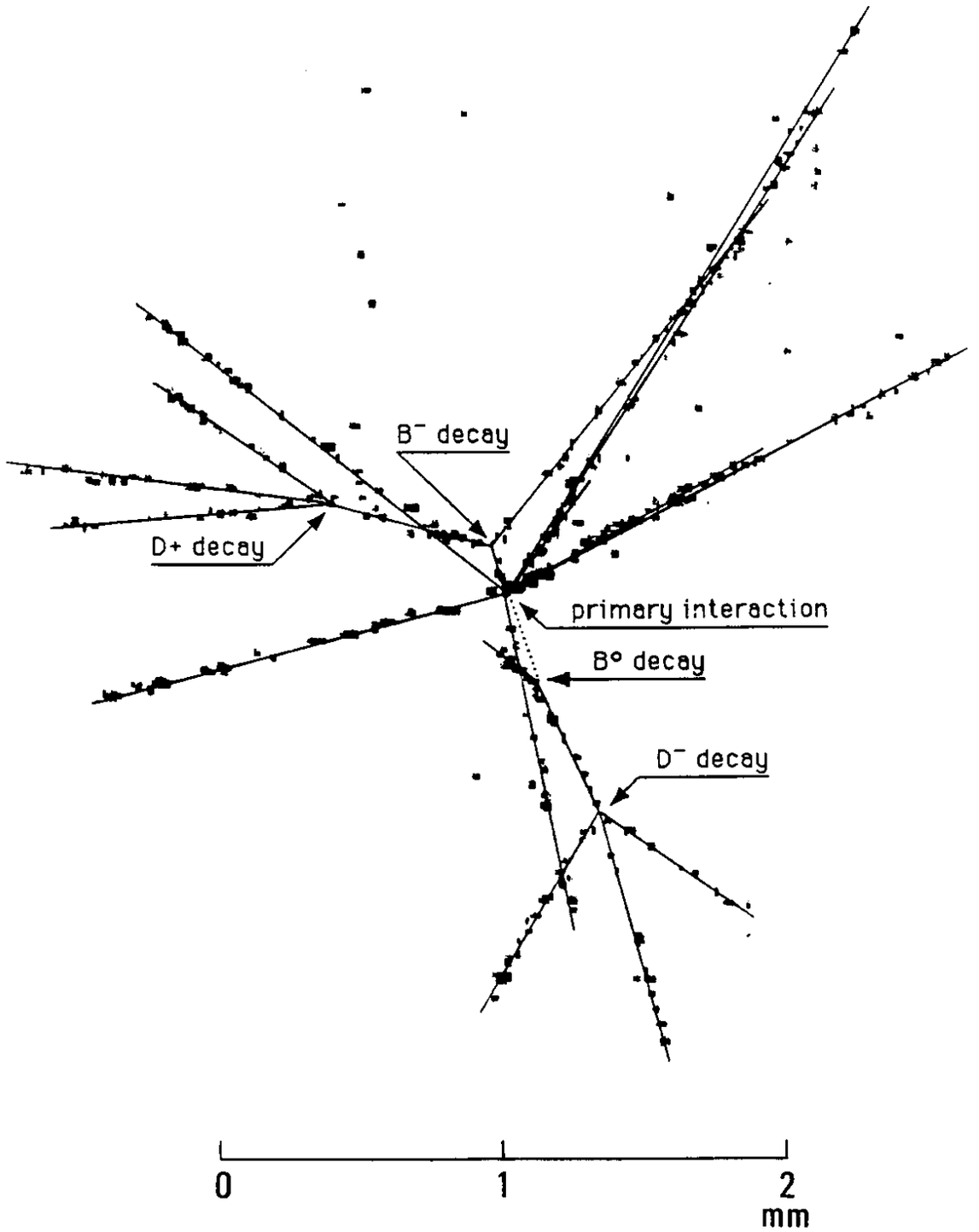


**Fig. 6**

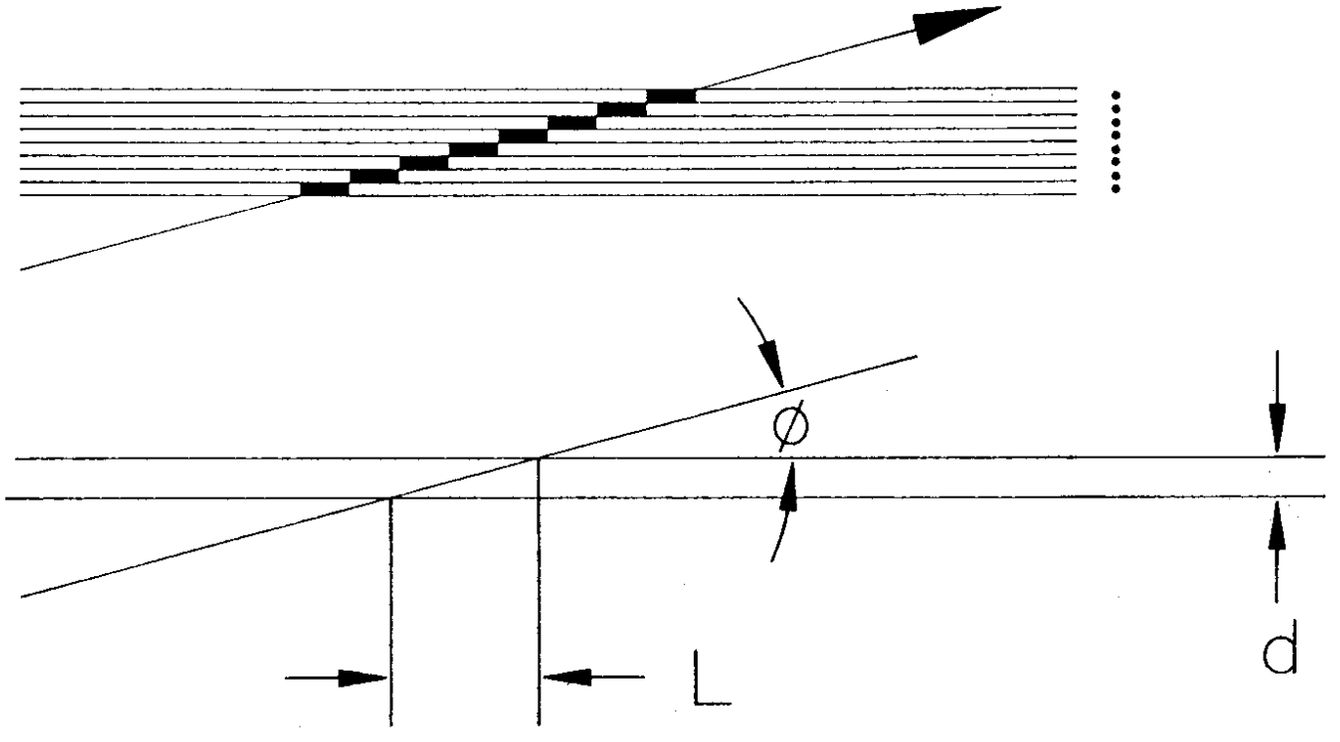


$$\text{LIGHT} \propto L \propto d/\sin \phi$$
$$\sin \phi \sim \tan \phi \sim 1/\gamma_c$$
$$\text{LIGHT} \propto d.\gamma_c$$

**Fig. 7**

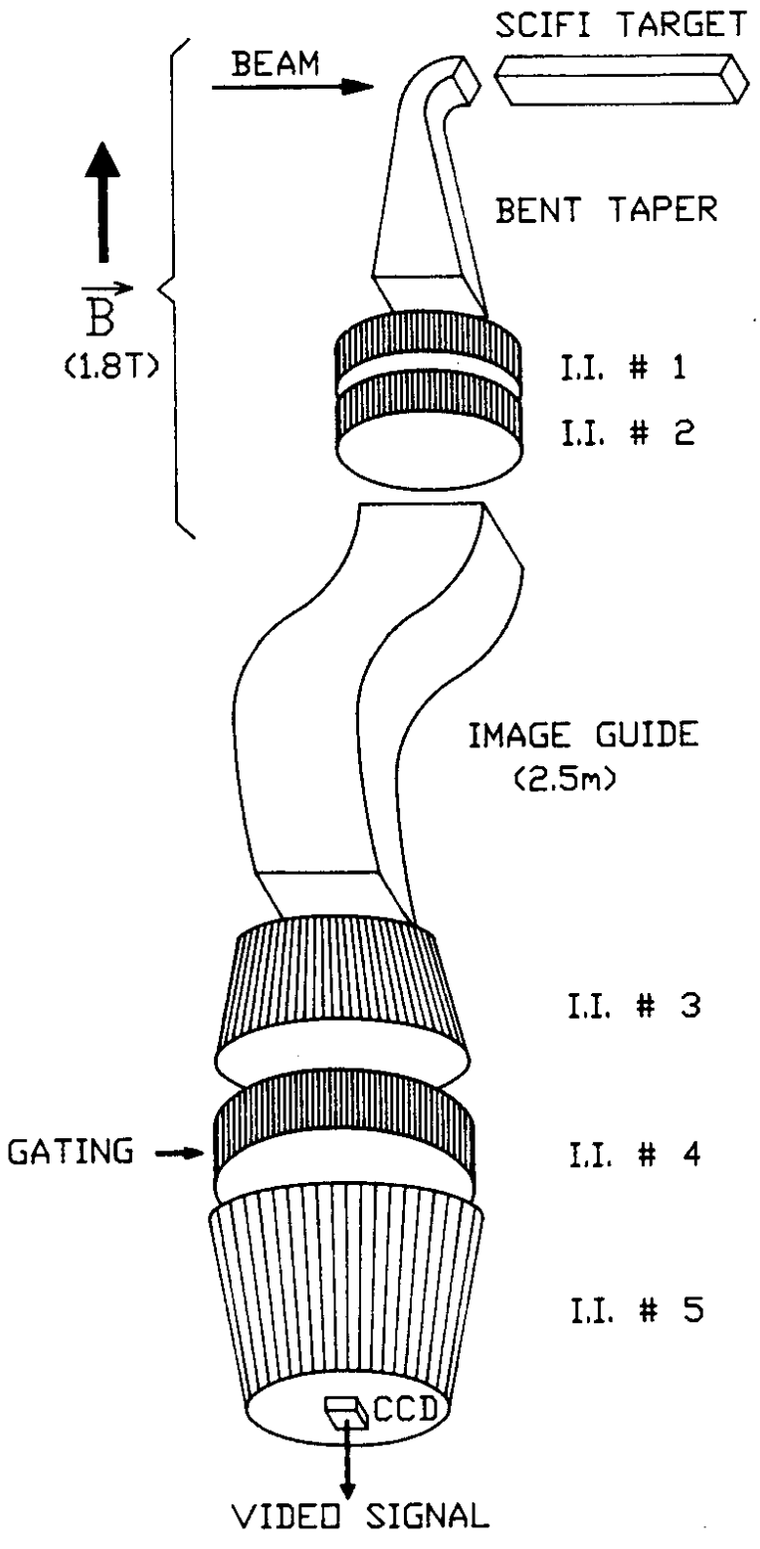
SCIFI TARGET
BEAM
BENT TAPER
B
(1.8T)
I.I. # 1
I.I. # 2
IMAGE GUIDE
(2.5m)
I.I. # 3
GATING
I.I. # 4
I.I. # 5
CCD
VIDEO SIGNAL

**Fig. 8**

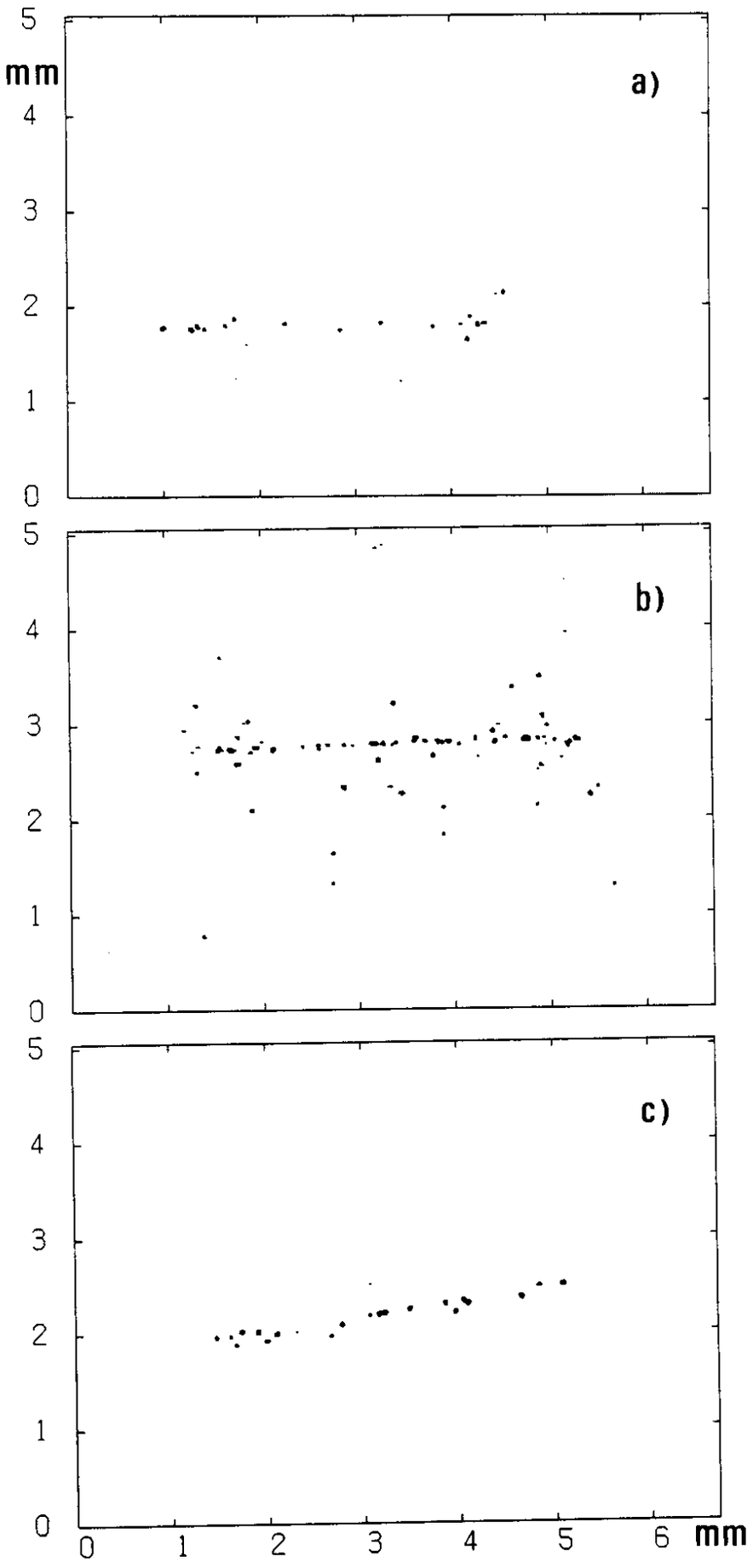


Fig. 9

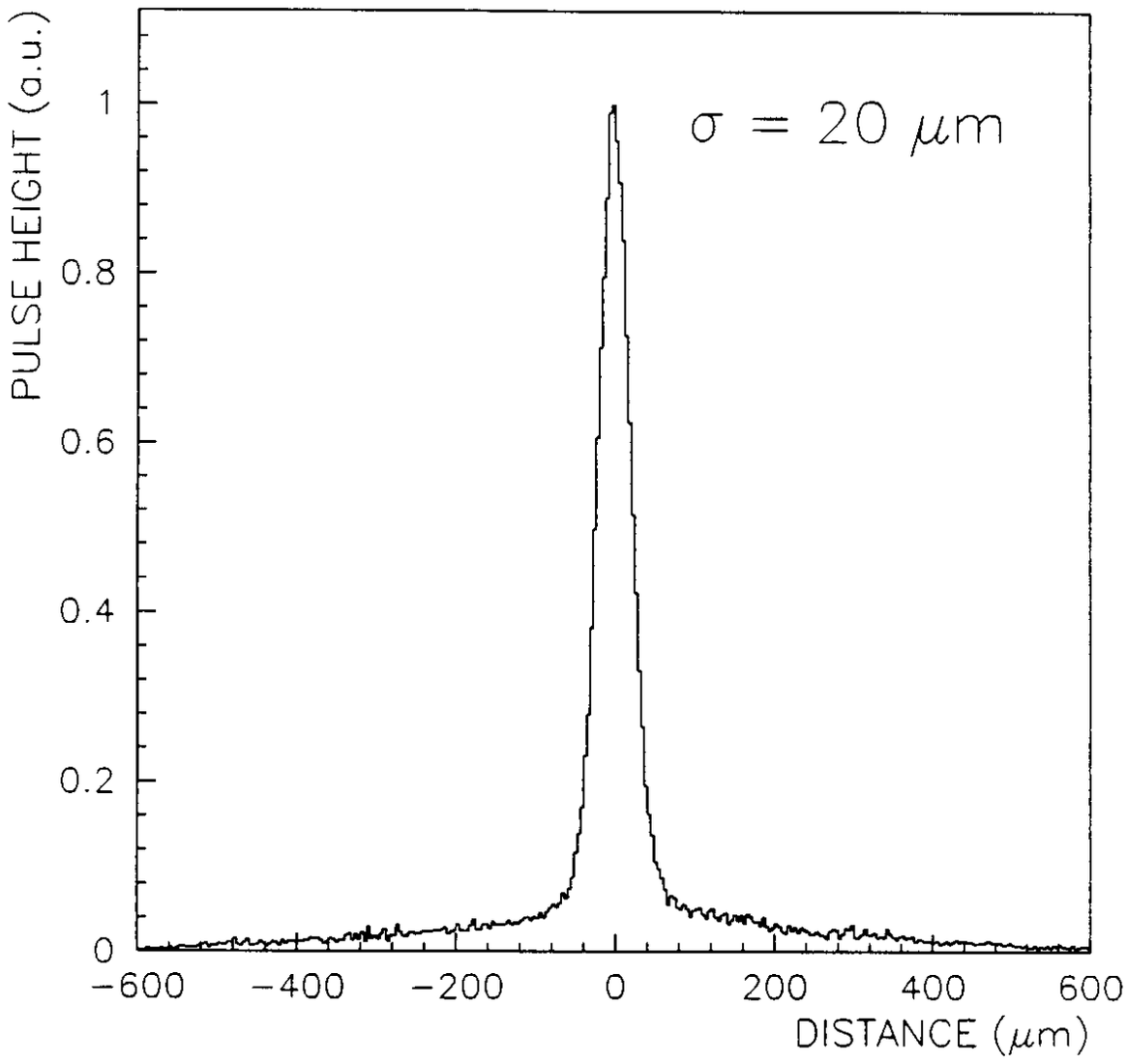
PULSE HEIGHT (a.u.)
1
0.8
0.6
0.4
0.2
0
σ = 20 μm
−600
−400
−200
0
200
400
600
DISTANCE (μm)

**Fig. 10**

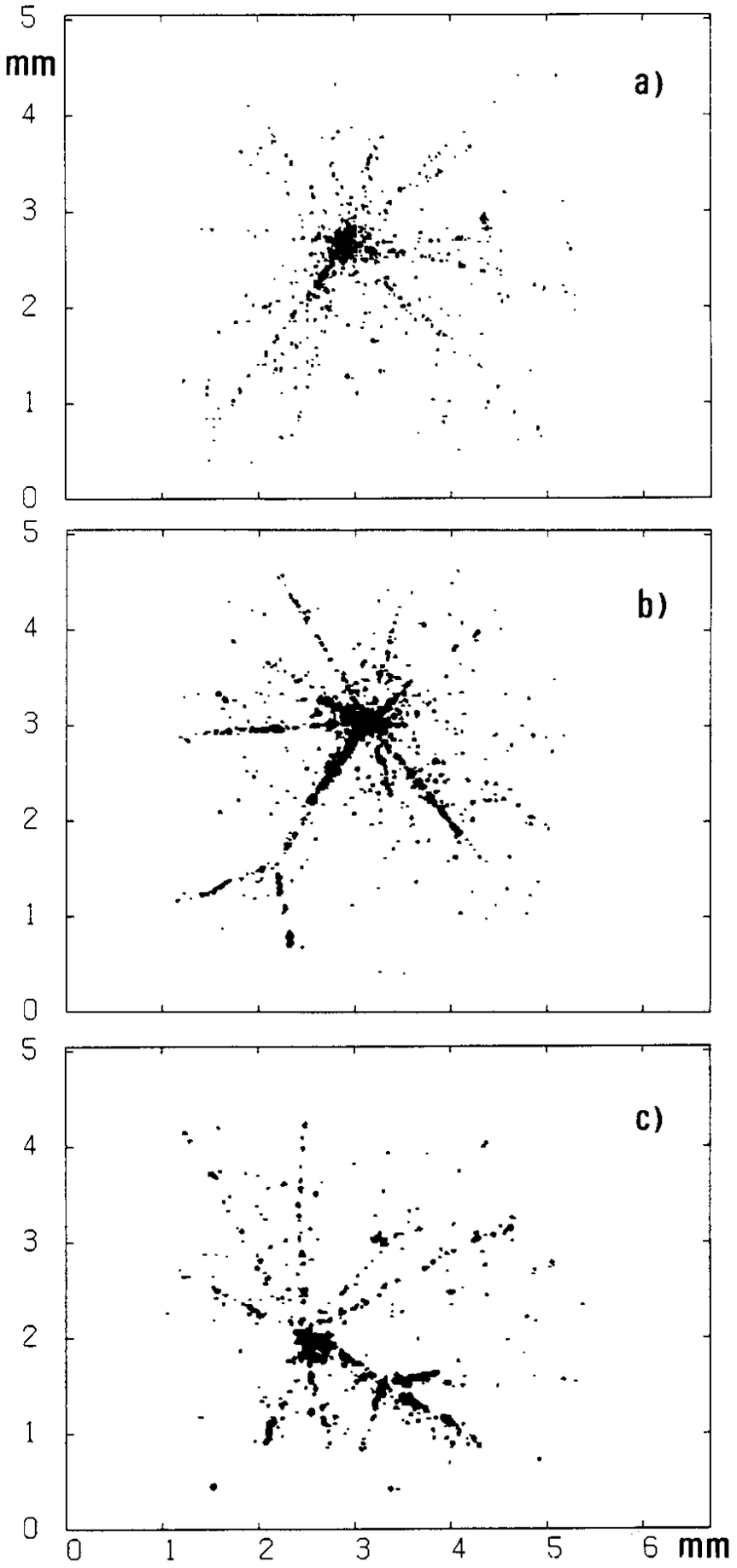


**Fig. 11**